Effects of Biofilm Structures on Oxygen Distribution and Mass Transport

Dirk de Beer, Paul Stoodley, Frank Roe, and Zbigniew Lewandowski*
Center for Biofilm Engineering, Montana State University, Bozeman, Montana 59717

Received September 17, 1993/Accepted December 14, 1993

Aerobic biofilms were found to have a complex structure consisting of microbial cell clusters (discrete aggregates of densely packed cells) and interstitial voids. The oxygen distribution was strongly correlated with these structures. The voids facilitated oxygen transport from the bulk liquid through the biofilm, supplying approximately 50% of the total oxygen consumed by the cells. The mass transport rate from the bulk liquid is influenced by the biofilm structure; the observed exchange surface of the biofilm is twice that calculated for a simple planar geometry. The oxygen diffusion occurred in the direction normal to the cell cluster surfaces, the horizontal and vertical components of the oxygen gradients were of equal importance. Consequently, for calculations of mass transfer rates a three-dimensional model is necessary. These findings imply that to accurately describe biofilm activity, the relation between the arrangement of structural components and mass transfer must be understood.
Key words: confocal microscopy • microelectrodes • cell clusters • pores

INTRODUCTION

Surfaces immersed in water under physiological conditions are rapidly covered with biofilms, which consist of microorganisms embedded in a matrix of extracellular substance (EPS).[8] Intensive research is in progress to elucidate the influence of biofilm activity on a variety of industrial,[7,8,10] medical,[2,30] and environmental[20,28,32] processes.

Substrate conversion rates in biofilms are controlled by growth kinetics and mass transport processes. Various conceptual and mathematical models have been proposed to describe the structure and function of biofilms.[8,23,29] These models describe biofilms as planar structures with homogeneous cell distribution. Mass transfer through the mass boundary layer and within the biofilm is assumed to be diffusional and perpendicular to the surface to which it is attached (the substratum). However, microscopic observations indicate that biofilms are not flat and the distribution of microorganisms is not uniform. Instead, multispecies biofilms form highly complex structures containing "voids," "channels," "cavities," "pores," and "filaments," with cells arranged in "clusters" or "layers." Such complex structures were found in a wide variety of biofilms such as methanogenic films from fixed-bed reactors,[24] aerobic films from wastewater plants,[9,19] nitrifying biofilms,[16] and pure culture biofilms of *Vibrio paraheamolyticus*[17] and *Pseudomonas aeruginosa*.[27]

It has been hypothesized that the biofilm structure is not a chance occurrence but represents an optimal arrangement for the influx of nutrients; however, no direct evidence had been presented.[17,24] The effective diffusion coefficient in aerobic biofilms was found to be dependent on flow conditions and biofilm structure, indicating convection through pores in the biofilm.[25] Voids might enhance substrate and product fluxes throughout the biofilm by decreasing diffusional resistance or by facilitating convection. This implies that the substrate concentration in voids will be higher than that in adjacent biomass. To verify this, substrate concentrations in voids and cell clusters of physiologically active biofilms under flow conditions must be measured directly. Therefore, we integrated confocal scanning laser microscopy (CSLM) and microelectrode techniques to assess the relationship between the internal structure of biofilms and oxygen concentration profiles. CSLM enhances visualization of biofilm structures by eliminating the interference from out-of-focus objects.[5,31] No preparatory steps are needed; observations can be done under growth conditions, while the biofilm remains physiologically active. Oxygen microelectrodes allow local concentrations to be measured with minimal disturbance of the biofilm structure.[4,18,22]

The simplistic conceptual model of biofilm structure commonly accepted for mathematical modelling of biofilm activity raises serious doubts because it does not reflect the complexity of the biofilm structure. The goal of this study was to determine the relationship between structure and mass transfer in biofilm systems.

MATERIALS AND METHODS

Biofilm Development

Biofilms were grown using a minimal salt medium consisting of KH_2PO_4 (2.2 m*M*), K_2HPO_4 (4 m*M*), $(NH_4)_2SO_4$ (0.76 m*M*), $MgSO_4$ (4.1×10^{-2} m*M*), and glucose (2.2 m*M*), made up with distilled water and with a resulting pH value of 7. A continuous culture reactor, consisting of a flow cell with recycle loop, was inoculated with an undefined consortia of detached cells from a mature biofilm. During the initial 6 h the reactor was run in a batch mode to allow colonization of the coverslip. Subsequently, the reactor was switched to continuous culture with a liquid

* To whom all correspondence should be addressed.

CCC 0006-3592/94/0111131-08

residence time of 26 min. The culture temperature during growth and measurements was 20 ± 1°C. During growth a recycle rate of 5.4 mL/s was maintained, resulting in a liquid velocity in the flow cell of 0.09 m/s. The flow cell (Fig. 1) was a polycarbonate channel with a 0.6 × 1.0-cm cross section and a glass coverslip top, which served as an observation window. A cyclone air–liquid separator placed in the recycle loop allowed complete mixing, aeration, and separation of gas bubbles from the reactor liquid. During biofilm growth and measurements the channel was completely filled with medium. The flow cell, connected to the support system with flexible tubing, could be mounted on a microscope stage. The biofilms developed on the coverslip were accessible for in situ microscopic examination and measurements with specially designed oxygen microelectrodes.

Microelectrode Measurements

The oxygen microelectrodes used were similar to those described previously;[21] however, instead of being linear the devices were bent in a "J"-shape (Fig. 1). With a heating coil the glass was softened locally and bent with a stiff metal wire to a 90° angle, first at 3 mm and then at 43 mm from the tip. Subsequently, the electrode tips were slightly recessed in freshly prepared 3 *M* KCN, rinsed in distilled water and acetone, dried with a hot air gun for 3 min, and covered with fresh DPX. The resulting electrodes with tip diameters of 7 to 15 μm showed a normal response and negligible stirring sensitivity (<2%). The "J" shape allowed the electrodes to be introduced into the flow cell with the tip raised to the coverslip, thus allowing oxygen concentration profile measurements made in a vertical direction, from the channel center to the coverslip covering the flow cell.

The biofilm of interest was attached to the underside of the glass coverslip. Positioning the tip in the vertical direction was done using a micromanipulator with a stepper motor, with an accuracy of 1 μm. The amplified microelectrode signals and relative positions were recorded using a data acquisition system and stored for later processing.

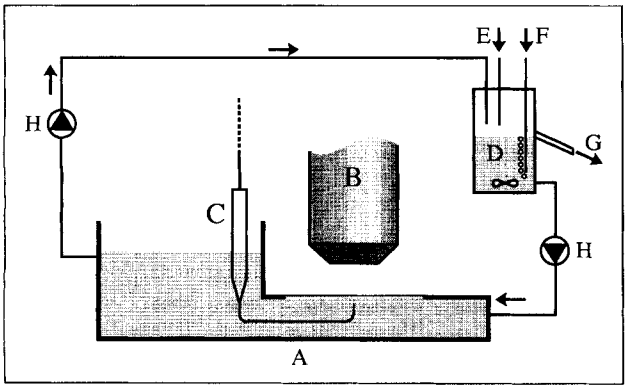

Figure 1. Schematic of experimental setup: (A) flow cell; (B) microscopic objective; (C) J-shaped microelectrode; (D) mixing vessel; (E) nutrient solution; (F) air supply; (G) waste outlet; (H) recirculation pumps.

Determination of the relative position of the microelectrode with respect to the glass surface was performed with conventional light microscopy. Oxygen profiles were measured at 80-μm intervals along transects, ranging form 500 to 1000 μm in length, traversing both pores and clusters at various locations in a biofilm. A regular matrix of data points was constructed from the profiles by linear interpolation. Subsequently, contour plots were made with an overlay of vectors representing the local gradients using the commercially available software package MATLAB. Oxygen diffusion fluxes in the pores and to cell clusters were calculated from the concentration profiles using Fick's law,

$$J = D \cdot dc/dx \qquad (1)$$

where J is the flux, D the diffusion coefficient, and dc/dx the oxygen gradient. Here D was assumed to be 2.27×10^{-9} m^2/s at 20°C. This value was obtained after a temperature correction of the literature value[1] using the Stokes–Einstein relation.[26]

Microscopic Analyses

For analysis of the structure of the biofilm a Bio-rad MRC600 confocal scanning laser (Kr/Ar) system with an Olympus BH2 light microscope and a MS plan 20 IC objective was used. Four CSLM techniques were used for imaging: (1) Reflected laser light of combined 488, 546, and 647 nm wavelengths was used to observe biomass and microelectrodes. (2) Fluorescence exclusion with fluorescein (0.1 m*M*) was used to enhance visualization of internal structures.[6] (3) Fluorescent microspheres were used to investigate the permeability of the biofilms (Fluoresbrite Carboxylate microspheres 0.87 μm, Polysciences). The microspheres were added to the reactor (1.4×10^9 spheres/mL) 60 min prior to imaging to allow penetration in the biofilm. (4) Propidium iodide staining (10 mg/L, for 30 min) was used to distinguish individual cells. Additionally, extracellular polymeric substances were visualized by light microscopy after staining with Alcian blue (0.1%) for 30 min.[13]

RESULTS

After inoculation, the glass surface became colonized in a few hours and a biofilm was formed after switching to continuous culture. Two days later cell clusters were observed approximately 80 μm thick and 100 to 300 μm in diameter. The clusters were separated by open spaces of 50 to 100 μm wide (Fig. 2). The clusters covered approximately 50% of the total surface of the glass slide. In the void areas the glass surface was covered with biofilm approximately 10 μm thick.

After 3 days, cell clusters were developed to a thickness of 140 to 160 μm that still covered about 50% of the surface. Three-day-old biofilms imaged with fluorescence exclusion at 0, 20, and 80 μm from the substratum showed

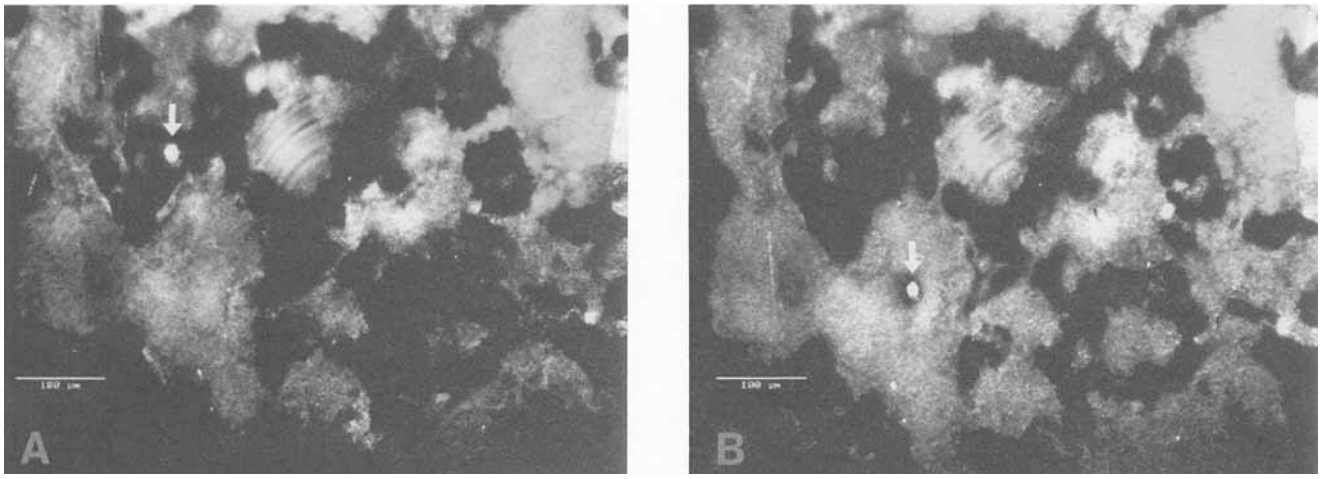

Figure 2. Biofilm structures by confocal imaging with reflected light. Cell clusters are shown as light areas against the darker void areas, near the base of an 80-μm-thick biofilm. The microelectrode tip is indicated with arrows in (A) a void and (B) a cell cluster. Bar: 100 μm.

that the larger cell clusters were not closely attached to the substratum (Figs. 3a–d). Voids of 20 to 40 μm were visible between the larger clusters (ca. 300 μm diameter) and the substratum. The clusters were attached to the substratum with strands. The smaller clusters were more closely or completely attached. Voids under cell clusters were not observed in 2-day-old biofilms.

After approximately 10 days biofilms developed to a thickness of approximately 600 μm, the maximal allowing confocal observations. Also in those mature biofilms voids were observed stretching from the biofilm surface to the substratum. The voids were often interconnected with channels parallel to the substratum. The accessibility of the voids was confirmed by adding fluorescent beads to the reactor. The beads penetrated the biofilm revealing a complex network of voids within the biofilm. The pattern of the beads followed closely the contours of the voids as visualized with fluorescein (Fig. 4). A part of the beads stuck to the walls of the voids; another part was immobilized in the main body of the voids seemingly attached to otherwise invisible strands.

Combined staining with propidium iodide and fluorescein showed that cells are exclusively located in the clusters (Fig. 5). Alcian blue caused irregular staining of the biofilm, showing blue patches in the cell clusters adjacent to the voids, whereas the voids themselves were not stained.

For convenience, the following terminology is used hereafter: (1) The term *vertical* will refer to the direction perpendicular to the substratum and *horizontal* to the direction parallel to the substratum; (2) "voids" are formed by the space between the dense cell clusters. Voids in the vertical direction are referred to as *pores* and the voids in the horizontal direction below the biofilm surface are *conduits*.

With microscopic guidance the tip of the oxygen microelectrode was positioned in the pores or into the cell clusters (Figs. 2A) of the 2–day-old biofilm. The thickness of the biofilm, measured as the distance from the top of the cell clusters to the substratum, was approximately 80 μm. The oxygen concentration in the bulk liquid was 0.16 mM. The profiles measured at the indicated positions, which were 120 μm apart, showed significant differences (Fig. 6A). The profiles show that at a given distance from the substratum the oxygen concentration in the pore is always higher than in the cell cluster. Oxygen penetrated only 30 μm into the cell clusters leaving the lower 50 μm anaerobic, whereas in the pore oxygen it penetrated to the substratum. The thickness of the mass boundary layer above the cell cluster was 40 μm and in the pore 55 μm. These measurements were repeated 12 times with consistent results.

Oxygen profiles measured in cell clusters of 3–day-old, 160-μm-thick biofilms (Fig. 6B) differed from those measured in 2-day-old biofilms. The profiles consistently showed that the concentration at the substratum was higher than that in the middle of the cell cluster. This phenomenon was observed in all 31 oxygen profiles measured in cell clusters. The oxygen profiles in the pores were similar to those measured in the pores of an 80-μm-thick, 2-day-old biofilm (Fig. 6A).

Oxygen profiles measured in 3-day-old biofilms were used to construct cross-sectional contour plots. In three separate experiments, oxygen profiles were measured along eight transects of 500 to 1000 μm long, with comparable results. The oxygen concentration in the bulk was 0.15 to 0.16 mM. A representative contour plot was constructed from 11 oxygen profiles (Fig. 7). Comparison of the oxygen contours with the position of the cell clusters shows that the oxygen concentration is strongly correlated with the biofilm structure. The values of the mass boundary layer thickness were the same as those measured from the 2-day-old biofilm. Also the contour plot shows that the lowest oxygen concentrations can be found in the middle of the cell cluster. The arrows in the contour plot mark the direction of the local oxygen gradients; their lengths indicate the magnitude of the gradients. Oxygen concentration gradients were

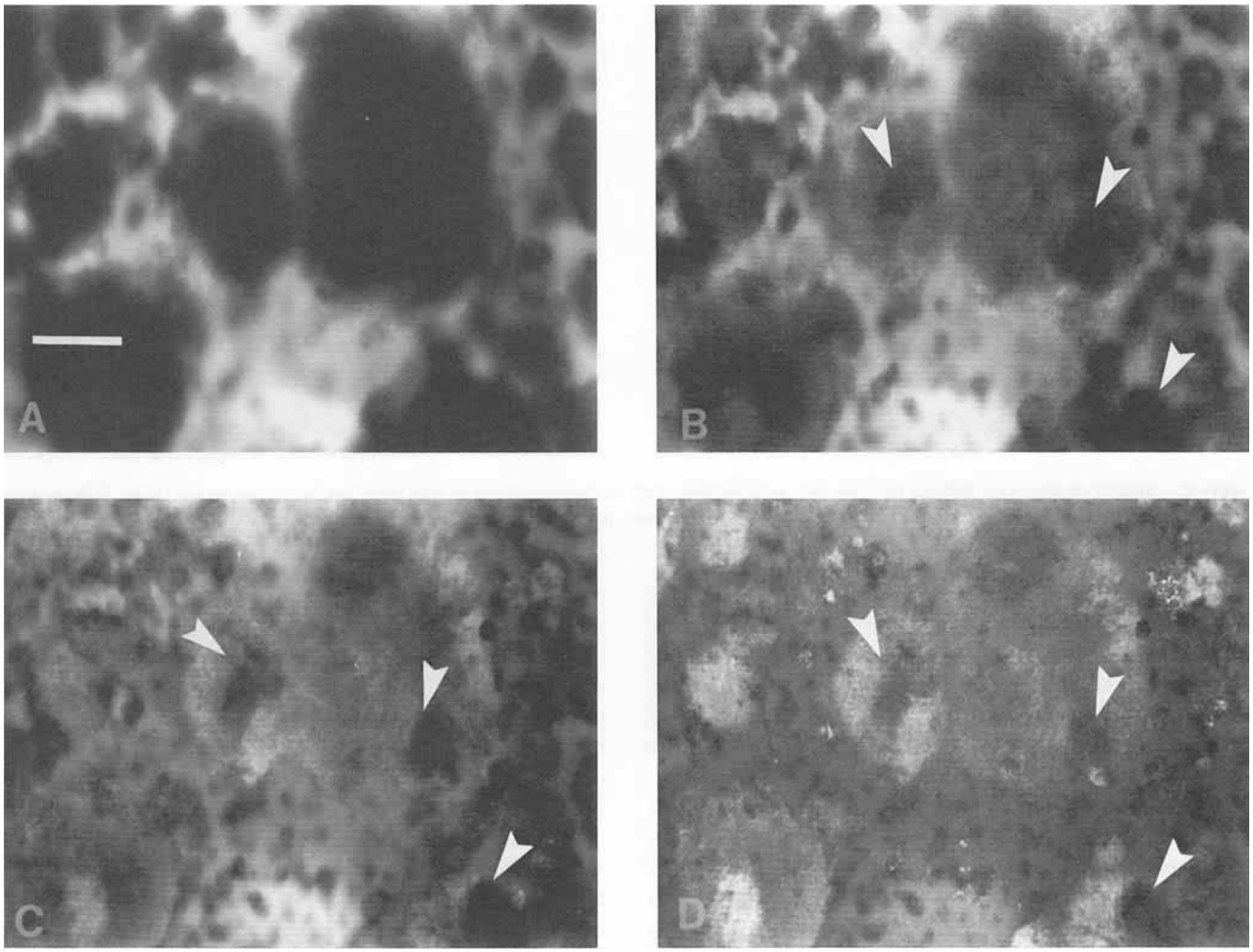

Figure 3. Biofilm structures imaged with confocal fluorescence exclusion microscopy. The 160-μm-thick biofilm was optically sectioned at various distances from the substratum: (A) 80 μm, (B) 40 μm, (C) 20 μm, and (D) at the substratum surface. The cell clusters are clearly seen at the 80- and 40-μm depths as dark areas, against a fluorescing light background of voids (A, B). Voids were also present underneath the cell clusters, as indicated by fluorescence at the 20-μm depth and at the substratum (C, D). Dark column-like structures connecting the cell clusters to the substratum, indicated by arrows, can be followed through the depth of the film. Bar: 100 μm.

normal to the cell cluster interface and pointed inward, as shown by the vectors. This indicates that oxygen is supplied to the cell cluster through all cell cluster–liquid interfaces. The largest gradients existed at both the cell cluster–pore liquid interface and the cell cluster–bulk liquid interface. The smaller gradients at the cell cluster–conduit interface indicated additional oxygen transport from the conduit to the cell cluster.

DISCUSSION

The confocal images of biofilms, unaffected by preparatory techniques such as dehydration, showed the presence of an extensive network of voids. Few other reports show biofilms with comparable structures, possibly because of structural deformation caused by embedding and sectioning techniques. However, the existence of an intricate system of channels has been demonstrated in anaerobic biofilms.[24] The pores had a diameter of about 50 μm and extended through most of the biofilm. Methanogenic biofilms produce vast amounts of gas, which might have caused the sponge-like structure. In aerobic biofilms no such extensive channeling has been reported.

Biofilms from trickling filters showed volcano-shaped bacterial colonies on the surface; the hollow cores supposedly facilitated transport of oxygen and nutrients through the colony.[19] Furthermore, in these films bacteria-grazing protozoa were observed wandering through the deeper layers of the biofilm, which indicates the existence of channels, although they were not observed directly. Using transmission electron microscopy channels were shown with a diameter of 1 μm in pure-culture aerobic biofilms of 3 to 10 μm thick.[9] The above-mentioned observations were done with light or electron microscopy using thin sectioning techniques.

This study demonstrated with CSLM techniques that the presence of voids are characteristic in aerobic biofilms as thick as 600 μm. It should be noted that preparatory

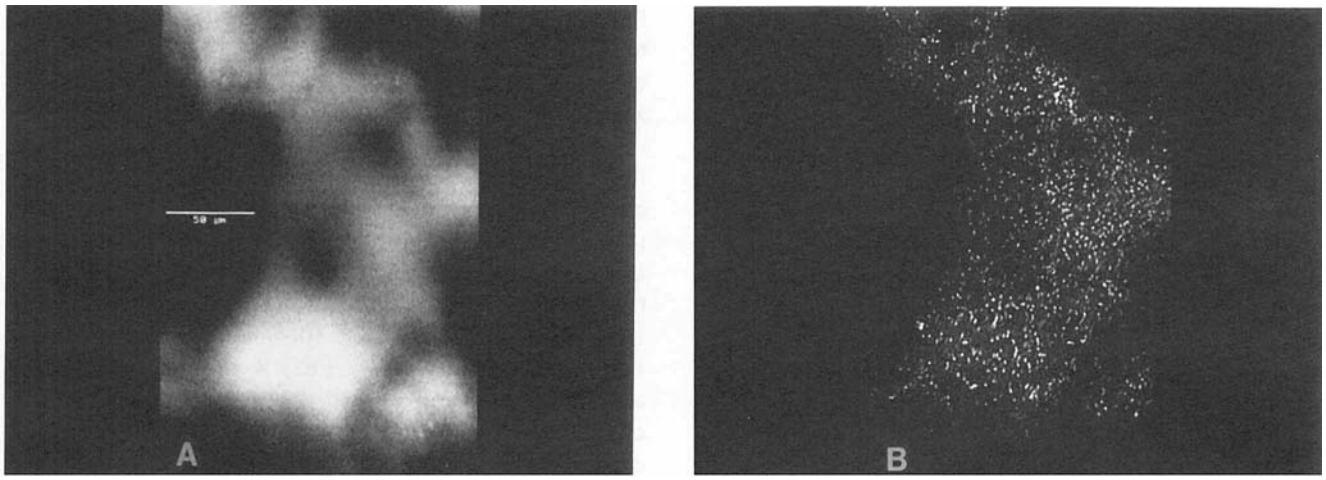

Figure 4. Void imaged by (A) fluorescence exclusion and (B) fluorescent beads of 1 μm.

techniques such dehydration and cryo-embedding, distort the biofilm structure considerably and cause the voids to close (data not shown).

The different CSLM techniques used revealed the actual complexity of the biofilm structure. Biofilms envisaged with confocal microscopy using fluorescein show cell clusters as dark areas, either because they are less accessible for fluorescein or because the fluorescence is quenched within the cell clusters. Propidium iodide staining revealed that cells are located almost exclusively in clusters. The fluorescent 1-μm latex beds can penetrate the voids between these clusters but not the cell clusters themselves. The beads indicated the presence of strands in the voids, possibly EPS of very low density. These strands could not be made visible with Alcian blue, but the cell clusters adjacent to the voids were stained intensively.

These observations lead to a new conceptual model of biofilms—a conglomerate of cell clusters that are more or less suspended but are attached to the substratum and each other with polymeric material (Fig. 8). The space between the cell clusters forms vertical and horizontal voids, making up a considerable component of the total biofilm volume. The cell clusters are microbial aggregates cemented with EPS, whereas the voids are open structures not clogged with EPS. This model has profound consequences for the understanding of substrate and product transport.

The differences between oxygen profiles measured in pores and cell clusters clearly show that a single microprofile may not be representative of a biofilm. A two-dimensional contour plot obtained from a series of profiles provides a more realistic representation of the oxygen distribution.

From the oxygen profiles in 80-μm-thick biofilms (Fig. 4) oxygen fluxes in vertical direction were calculated. The flux in the pore was 6.5×10^{-6} mol/m^2 · s and across the biomass/bulk liquid interface of the cell cluster 7.6×10^{-6} mol/m^2 · s. It can be recognized from the profiles in the pores and the cell clusters that oxygen concentration differences in the direction parallel to the substratum also exist, leading to fluxes in the horizontal direction. The

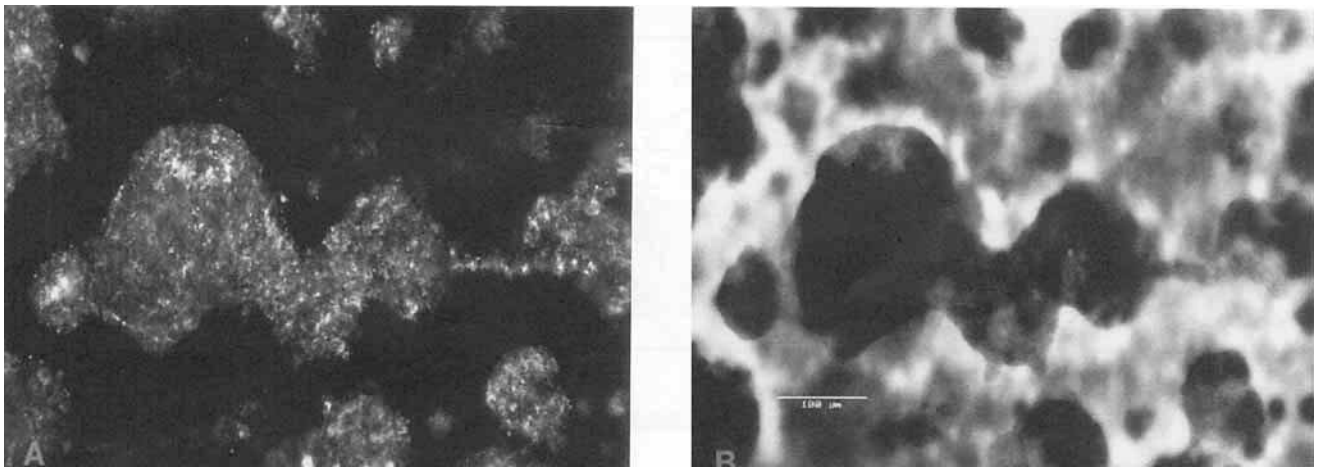

Figure 5. Cell clusters imaged with (A) propidium iodide and (B) fluorescence exclusion.

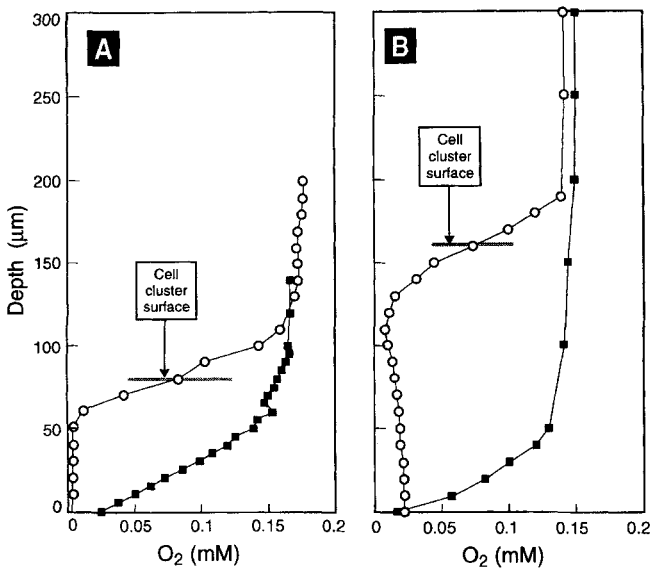

Figure 6. Oxygen concentration profiles measured in (■) a pore and (○) cell cluster in a biofilm of (A) 2 and (B) 3 days old.

horizontal distance between the measured concentration profiles was approximately 120 μm. From this and the concentration differences at equal depths between the profiles, the minimum horizontal fluxes were calculated. The fluxes from the void to the cell cluster are depth dependent and range from 0.54×10^{-6} to 2.7×10^{-6} mol/m^2 · s, with an average of 1.7×10^{-6} mol/m^2 · s. This is of the same order as the vertical fluxes from the bulk liquid to the cell cluster.

From the concentration profiles in Figure 7, oxygen fluxes were determined in horizontal and vertical directions. The average horizontal component of the local fluxes at each of the pore–cell cluster interfaces (x = 40, 200, 300, 380, and 740 μm; see Fig. 7) were calculated. The resulting five values were used to calculate the average horizontal flux from pores to cell clusters over the entire transect. The average horizontal flux to the cell clusters amounted to $1.85(\pm 0.27) \times 10^{-6}$ mol/m^2 · s. The vertical fluxes from the bulk liquid to the cell clusters amounted to $4.32(\pm 1.62) \times 10^{-6}$ mol/m^2 · s. Assuming the cell cluster to be a cylinder with a diameter of 300 μm and a height of 160 μm, the vertical mass flow rate per cell cluster was 3.0×10^{-13} mol/s and the horizontal mass flow rate was 2.78×10^{-13} mol/s. This indicates that the oxygen transport from the pore into the cell cluster is of the same order of magnitude as that directly from the bulk liquid into the cell cluster. This is further supported by the observation that the oxygen fluxes from the bulk liquid into the pores [$7.0(\pm 1.62) \times 10^{-6}$ mol/m^2 · s] and directly into the cell cluster [$4.32(\pm 1.62) \times 10^{-6}$ mol/m^2 · s] are approximately the same and that the pores and the cell clusters have equal surface coverage. Oxygen supply to cell clusters through the conduits was insignificant as compared with the transport from the pores and the bulk, as can be seen from the vectors in Figure 7. The oxygen profiles in cell clusters (Fig. 6B) show that the consumption rate along the upper surfaces of the cell cluster was higher than at the base. This indicates a heterogeneous distribution of cell densities or bacterial species within the cell clusters.

Initially, the cell clusters were seen to be adhered directly to the substratum, but after the thickness had increased to 160 μm, conduits beneath the clusters were formed. This explains the differences between the profiles in an-80-μm thick cell cluster, in which the oxygen concentration at the substratum was zero (Fig. 6A), and a 160-μm-thick cell cluster, showing the lowest oxygen concentration in the middle of a cluster and a higher concentration at the substratum (Fig. 6B). The oxygen at the base of cell clusters must originate from the adjacent pore. It is concluded that the conduits facilitated oxygen transport below the cell cluster in the horizontal direction, although the magnitude of this transport was small.

The presented observations on the structure of aerobic biofilms corroborate with the conclusions from a study on diffusion through acidogenic biofilms in the vertical direction of the surface.[14] It was found that the tortuosity amounted to 1 and the void fraction to 0.66, which implicates that the transport channels were linear, stretching

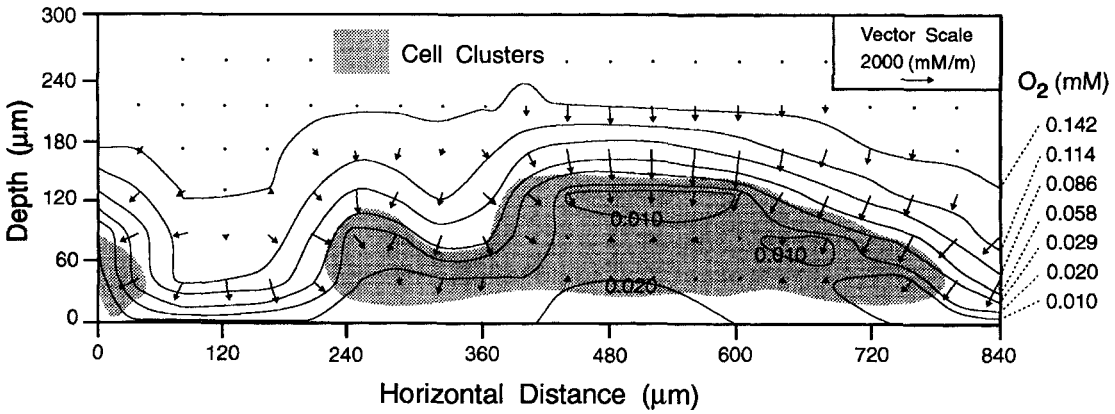

Figure 7. Oxygen contours and local gradients (represented by vectors) in a cross section of a 160-μm-thick biofilm. The positions of the cell clusters, shown as shaded areas, were determined by microscopic observation. Numbers within the figure and on the right margin indicate the local oxygen concentrations (*mM*).

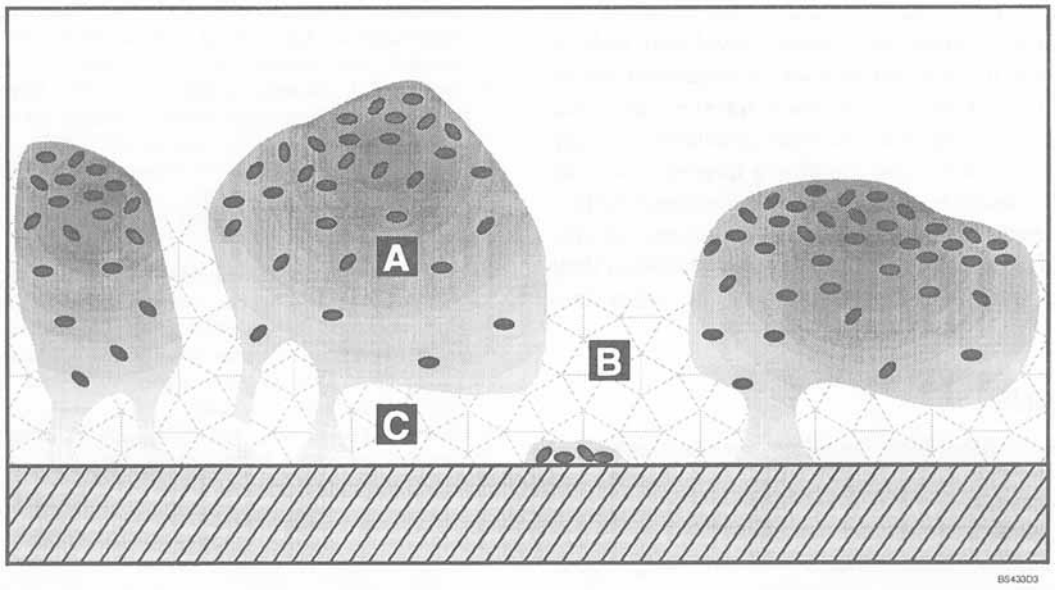

Figure 8. Conceptual model of biofilm: (A) cell cluster, (B) pore, (C) conduit.

from the bulk to the base of the biofilm, covering 66% of the biofilm surface. The observed pores in our study are straight, vertically oriented voids, covering approximately 50% of the surface.

The mass boundary layer followed the surface of the biofilm closely. The height of the cell clusters ranged between 80 and 160 μm, whereas the thickness of the mass boundary layer derived from the oxygen profiles was 40 to 55 μm. This implies that the exchange area is increased by the irregularities of the surface. Assuming cell clusters to be cylindrical with a radius (R) of 150×10^{-6} m and a height (h) of 160×10^{-6} m, covering a fraction (α) of 0.5 of the substratum surface (A_s) that is also covered with a thin biofilm in between the cell clusters, the biofilm surface (A_b) is twice that of the substratum surface, since $A_b/A_s = 1 + 2 \cdot \alpha \cdot h/R$. Studies on sediments demonstrated that surface elements must have a height of at least 50% of the mass boundary layer to have an influence on the shape of the mass boundary layer.[15] At lower velocities, the mass boundary layer will be thicker and may not follow the contours of the biofilm. The exchange area then will be equal to the substratum area.

Biofilms appear to be nonuniform structures consisting of discrete cell aggregates and interstitial voids which facilitate oxygen transport. This description has analogies with that of porous media which exhibit primary and secondary porosities.[3,11] Diffusion through cell clusters can be associated with the primary porosity and transport through voids with secondary porosity. This model has profound consequences for the understanding of mass transport processes in biofilms. The resistance to mass transfer in both cell clusters and interstitial voids must be assessed for the mathematical modeling of transport rates through the biofilm and into cell clusters; the use of one transport parameter, such as the effective diffusion coefficient,[25] is insufficient. For example, in the case of biocide applications, the presence of biocide at the base of a biofilm does not necessarily mean that the cell clusters are entirely penetrated. It has been found that after treatment with biocide, regrowth and resumption of biofilm activity are remarkably fast.[12] This may be attributed to limited penetration of the biocide into the cell clusters, from which regrowth or recovery from injury occurs.

Mass transfer in biofilms is a much more complex process than previously thought. Typical biofilms are complex structures consisting of cell clusters, pores, and conduits. A strong relationship exists between the arrangement of these structures, substrate distribution, and transport in biofilms. The actual structure of a typical biofilm allows a higher transport rate from the bulk liquid and consequently a higher cell activity than a homogeneous planar structure, as traditionally assumed. Biofilm models based on the assumption of one-dimensional transport may underestimate the transport rate because the horizontal component is neglected, whereas the data presented here lead to the conclusion that the substrate supply to cell clusters in horizontal direction is significant. Moreover, voids may enhance mass transfer to the cells by facilitating convection through the biofilm.

The activity of a heterogeneous biofilm depends strongly on characteristics of the bulk liquid–biofilm interface: Does the boundary layer follow the irregularities of the biofilm or is it a layer parallel to the substratum? If it does follow the biofilm irregularities, as observed under the experimental conditions described here, the one-dimensional model is not sufficient. If the boundary layer becomes parallel to the substratum, which may happen at lower bulk liquid velocities, a one-dimensional model using an average mass transfer coefficient is probably sufficient to calculate the biofilm activity.

Models for heterogeneous biofilms have been proposed; however, these can be applied only for very thin cell layers

where gradients in the biofilms and lateral transport can be ignored. The multispecies models developed address the stratification of different species in horizontal layers as resulting from kinetics and mass transfer; however, the existence of horizontal chemical gradients strongly complicates the problem and requires a three-dimensional approach. We conclude that to better understand biofilm behavior in response to substrate concentrations, biocide treatment, and hydraulic regimes, the relation between their structure and transport phenomena must be taken into account.

CONCLUSIONS

1. Aerobic biofilms were found to have a highly heterogeneous structure consisting of cell clusters and voids. Cells were primarily located in the cell clusters, embedded an EPS matrix. The voids form a network of channels of pores connected with the bulk liquid. The void fraction was about 50%.
2. The oxygen distribution in the above the biofilm was strongly correlated with the biofilm structure. Diffusion into the cell clusters occurred from all interfaces with the surrounding liquid in a direction normal to the interface. The total diffusional substrate flux from the bulk liquid to the biofilm was increased by the irregularities of the biofilm surface.
3. For an accurate calculation of transport rate, under a wide range of flow regimes, a three-dimensional model is necessary.

The research was supported by the cooperative agreement ECD-8907039 between the National Science Foundation and Montana State University. The authors thank Brian Goldstein for his help with data processing.

References

1. Andrussow, L. 1969. Diffusion. In: Landolt-Börnstein Zahlenwerte und Functionen II/5a. Springer, Berlin.
2. Anwar, H., Strap, J. L., Costerton, J. W. 1992. Kinetic interaction of biofilm cells of *Staphylococcus aureus* with cephalexin and tobamycin in a chemostat system. Antimicrob. Agents Chemother. **36**(4): 890–893.
3. Baveye, P., Valocchi, A. 1989. An evaluation of mathematical models of the transport of biologically reacting solutes in saturated soils and aquifers. Wat. Resour. Res. **25**(6): 1413–1421.
4. de Beer, D., van den Heuvel, J. C., Ottengraf, S. P. P. 1993. Microelectrode measurements of the activity distribution in nitrifying bacterial aggregates. Appl. Environ. Microbiol. **59**: 573–579.
5. Caldwell, D. E., Korber, D. R., Lawrence, J. R. 1992. Confocal laser microscopy and digital image analysis in microbial ecology. Adv. Microbiol. Ecol. **12**: 1–67.
6. Caldwell, D. E., Korber, D. R., Lawrence, J. R. 1992. Imaging of bacterial cells by fluorescence exclusion using scanning confocal laser microscopy. J. Microbiol. Meth. **15**(4): 249–263.
7. Characklis, W. G., Little, B. J., Stoodley, P., McCaughey, M. S. 1991. Microbial fouling and corrosion in nuclear power plant service water systems. Proc. Corrosion '91 NACE, Cincinnati, OH.
8. Characklis, W. G., Marshall, K. C. 1990. Biofilms: A basis for an interdisciplinary approach. pp. 3–15 In: W. G. Characklis and K. C. Marshall (eds.), Biofilm. Wiley, New York.
9. Eighmy, T. T., Maratea, D., Bishop, P. L. 1983. Electron microscopic examination of wastewater biofilm formation and structural components. Appl. Environ. Microbiol. **45**: 1921–1931.
10. Ford, T., Mitchell, R. 1990. The ecology of microbial corrosion. Adv. Microbiol. Ecol., **11**: 231–262.
11. Freeze, R. A., Cherry, J. A. 1979. Groundwater. Prentice-Hall, Englewood Cliffs, NJ.
12. Griebe, T., Chen, C., Srinivasan, R., Steward, P. S. Analysis of biofilm disinfection by free monochloramine and free chlorine. In: G. G. Geesey, A. Lewandowski, and H.-C. Flemming (eds.), Biofouling/biocorrosion in industrial systems. Lewis, Chelsea, (to appear).
13. Hayat, M. A. 1975. Positive staining for electron microscopy. Van Nostrand Reinhold, New York.
14. Jian, Y., Pinder, K. L. 1993. Diffusion of lactose in acidogenic biofilms. Biotechnol. Bioeng. **41**(7): 736–744.
15. Jorgensen, B. B., Des Marais, D. J. 1990. The diffusive boundary layer of sediments: Oxygen microgradients over a microbial mat. Limnol. Oceanogr. **35**(6): 1343–1355.
16. Kugaprasatham, S., Nagaoka, H., Ohgaki, S. 1992. Effect of turbulence on nitrifying biofilms at non-limiting substrate conditions. Water Res. **26**(12): 1629–1638.
17. Lawrence, J. R., Korber, D. R., Hoyle, B. D., Costerton, J. W., Caldwell, D. E. 1991. Optical sectioning of microbial biofilms. J. Bacteriol. **173**(20): 6558–6567.
18. Lewandowski, Z., Walser, G., Characklis, W. G. 1991. Reaction kinetics in biofilms. Biotechnol. Bioeng. **38**: 877–882.
19. Mack, W. N., Mack, J. P., Ackerson, A. O. 1975. Microbial film development in trickling filters. Microbiol. Ecol. **2**: 215–316.
20. Ottengraf, S. P. P. 1989. Exhaust gas purification. In: H. Rehms and G. Reeds (eds.), Biotechnology, vol. 8, VCH-Verlaggesellschafft, Weinheim, Germany.
21. Revsbech, N. P. 1983. *In situ* measurement of oxygen profiles of sediments by use of oxygen microelectrodes. In: E. Gnaiger and H. Forstner (eds.), Polarographic oxygen sensors: Aquatic and physiological applications. Springer, Heidelberg.
22. Revsbech, N. P., Jorgensen, B. B. 1986. Microelectrodes: Their use in microbial ecology. Adv. Microbial Ecol. **9**: 293–352.
23. Rittmann, B. E., Manem, J. A. 1992. Development and experimental evaluation of a steady-state, multispecies biofilm model. Biotechnol. Bioeng. **39**: 914–922.
24. Robinson, R. W., Akin, D. E., Nordstedt, R. A., Thomas, M., Aldrich, H. C. 1984. Light and electron microscopic examinations of methane-producing biofilms from anaerobic fixed-bed reactors. Appl. Environ. Microbiol. **48**: 127–136.
25. Siegrist, H., Gujer, W. 1985. Mass transfer mechanisms in a heterotrophic biofilm. Water Res. **19**(11): 1369–1378.
26. Simpson, J. H., Carr, H. Y. 1958. Diffusion and nuclear spin relaxation in water. Phys. Rev. 2nd series, **111**: 1201–1202.
27. Steward, P. S., Peyton, B. M., Drury, W. J., Murga, R. 1993. Quantitative observations of heterogeneities in *Pseudomonas aeruginosa* biofilms. Appl. Environ. Microbiol. **59**(1): 327–329.
28. Tchobanoglous, G. 1992. Wastewater engineering: Treatment, disposal, reuse, 3rd edition. McGraw-Hill, New York.
29. Wanner, O., Gujer, W. 1986. A multispecies biofilm model. Biotechnol. Bioeng. **28**: 314–328.
30. Ward, K. H., Olson, M. E., Lam, K., Costerton, J. W. 1992. Mechanisms of persistent infection associated with peritioneal implants. J. Med. Microbiol. **36**(6): 406–413.
31. Wilson, T. 1990. Confocal microscopy. Academic, London.
32. Wuhrmann, K. 1972. Stream purification. In: R. Mitchell (ed.), Water pollution microbiology. Wiley-Interscience, New York.